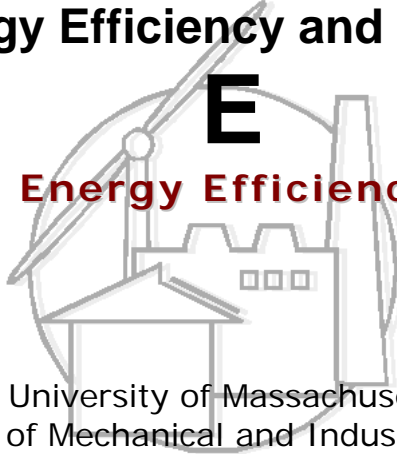


**Center for Energy Efficiency and Renewable Energy**

**C E E R E**

**Building Energy Efficiency Program**



University of Massachusetts  
Department of Mechanical and Industrial Engineering  
160 Governor's Dr.  
Amherst, MA 01003-9265

## **Progress Report**

### **Natural Convective Flow in Inclined Rectangular Glazing Cavities—3D study**

**Yunhua Yang**

**July, 2002**

# 1 Introduction

A number of two-dimensional numerical schemes were performed to study on the buoyancy flow inside the inclined glazing cavity in the pervious report, which included non-constant temperature boundary condition 2-D model, linearly time-dependent boundary condition 2-D model, periodically time-dependent boundary condition 2-D model and etc. However, because of the three-dimensionality of the flow characteristics, 2-D numerical models could not predict the heat transfer at small tilt angles, which leads to a prediction of a wrong transition angle of flow mode transition. The work in this report mainly focuses on three-dimensional numerical study in order to capture the 3-D characteristics of the flow in small tilt angle cavities.

## 2 Review of the Problem and Literature

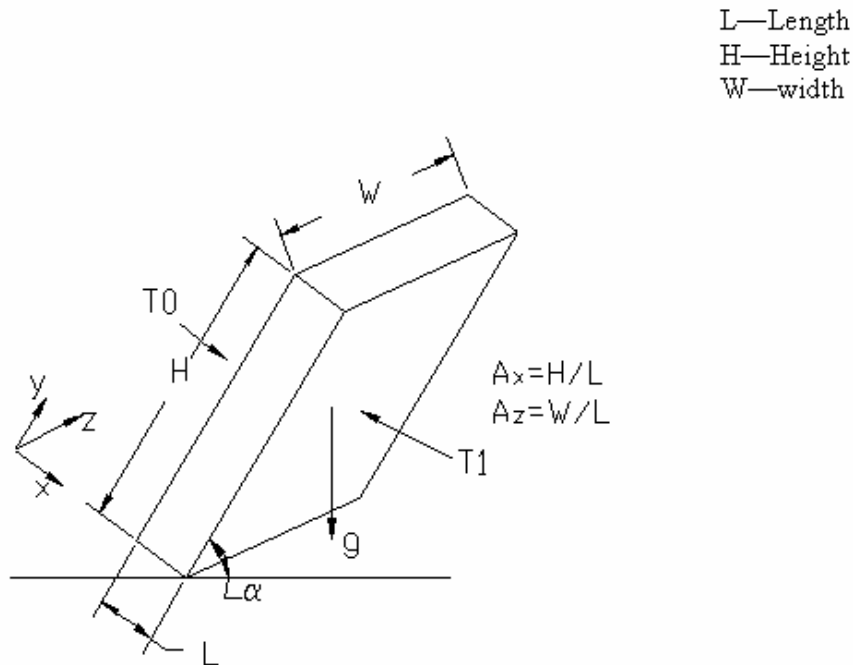


Figure 1: Geometry and Boundary Condition of the inclined cavity model

The detailed definition of geometry and the boundary conditions for the glazing cavity at a tilt orientation are given in the last report, so it is just briefly shown in Fig. 1, with higher temperature  $T_1$  and lower temperature  $T_0$ . The tilt angle is the one made by  $x=1$ (non-dimensional length) plane and the horizontal.

It is known from previous literature review on inclined buoyancy cavity flow that there exists a flow mode transition when the tilt angle changes from  $0^\circ$  to  $90^\circ$ . Between  $0^\circ$  and the transition angle, the flow consists of thermal instability-driven rolls, which makes the flow structure highly three-dimensional and thus complicated. In a rectangular cavity with different height ( $H$ ) and width ( $W$ ), the axes of the rolls are parallel to the shorter side. With the same height and width, the flow is more complicated, consisting of two series of superimposed rolls perpendicular to each other, which is called bimodal convection.

Three-dimensional numerical calculations have been carried out by Ozoe et al. (1983) and H.Q.Yang et al. (1986) at small tilt angles. Both of them carried out numerical studies using three-dimensional “cell” model. The basis of this cell model is assuming each of these convective cells, which aligns along the shorter side of the cavity, is confined to a rectangular volume, hereafter defined as a cell, whose dimensions do not change with the tilt angles. This assumption is based on the experimental observations. Thus, the single rectangular cell can be separated out to simulate, using the periodic boundary conditions at the neighboring boundary surfaces of the cell, and the results can be used to represent that of the whole cavity. One problem of this cell model is that the size of each cell is not known and needs to be assumed. Another problem lies in the unsteady nature of the flow at small angles. From the experiment of Symons and Peck

(1984), they found that when the cavity was rotated up to about  $15^\circ$ , the number of convective cells varied from 6 to 14 for a  $1 \times 6 \times 0.1667$  3-D cavity, for different experiments; and sometimes, even changing during one experiment.

Besides the cell model, three-dimensional whole cavity model, the calculation domain of which includes the whole cavity, was also performed in these papers, and the results showed good agreement with the experimental heat transfer data.

While flow at small tilt angle is always three-dimensional and cannot be predicted correctly by two-dimensional numerical models, flow at larger angles is two-dimensional, and simple two-dimensional model can work well, even for multicellular flow.

### **3 Three-dimensional Numerical Simulation Results**

#### ***3.1 Three numerical schemes with different initial conditions***

K.T. Yang (1988) pointed out in his review paper that, at a specific value of  $Ra$ , the buoyancy enclosure system is well defined and known, and the corresponding motions settle down eventually to a temporal asymptotic state, which maybe stationary, periodic, quasi-periodic, or chaotic. When the parameter  $Ra$  is changed to another value, the asymptotic state may also change to a different flow structure through a series of bifurcations. And these changes are very sensitive to the detailed spatial structure of the initial convection rolls, which in turn may depend on disturbances such as nonuniformities in geometry and boundary conditions, thermal history, and other experimental conditions.

Initial conditions are important in the aspect that it is one of the factors that determine the flow transition path. Given different initial conditions, the final state the

flow reaches might be different. The following three different initial velocity conditions are studied numerically.

### **3.1.1 Zero velocity initial condition model**

Zero velocity initial condition model applies a zero velocity at time=0 everywhere in the cavity. This is an ideal initial condition. The problem of this method is sometimes the flow doesn't start its motion because there is not enough initial perturbation.

### **3.1.2 Initial-cell model**

This method applies a number of initial convective cells inside the cavity to give the flow an initial perturbation for further motion. However, the unknown convective cell size is the main problem of this method.

### **3.1.3 Random velocity initial condition model**

This method uses the random number generator to generate random and small velocity components at each node. It is more close to the realistic experimental condition. In real situations, the fluid particles are constantly moving, and the boundary conditions are not ideal. These conditions can be modeled using random initial velocity field.

## **3.2 Results**

### **3.2.1 1x2x6 cavity, with Ra=30000**

This case was studied in H.Q.Yang(1986), and their calculated overall Nusselt number at the hotwall is 3.384 without mentioning initial conditions in their paper.

1). Zero initial velocity

With initial zero velocity, the velocity vector plot at timestep=600 shows only 4 cells in Fig. 2.

2). Initial-cell model

With 6 initial-cells defined for the initial condition, the velocity vector plot shows 6 cells in Fig. 3.

When applying 4 initial-cells, 4 final cells were formed; however, when the rotation direction of the 4 initial-cells was reversed, 6 cells were formed finally.

When applying 8 initial-cells, the behavior is similar to that of applying 4 initial-cells.

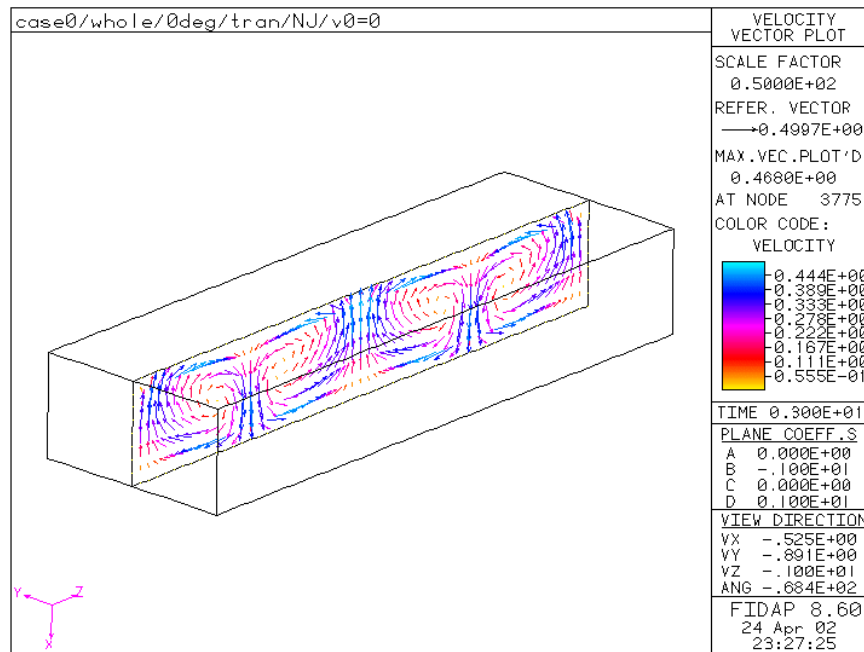


Figure 2. Velocity Vector Plot at Timestep=600 for initial zero velocity model

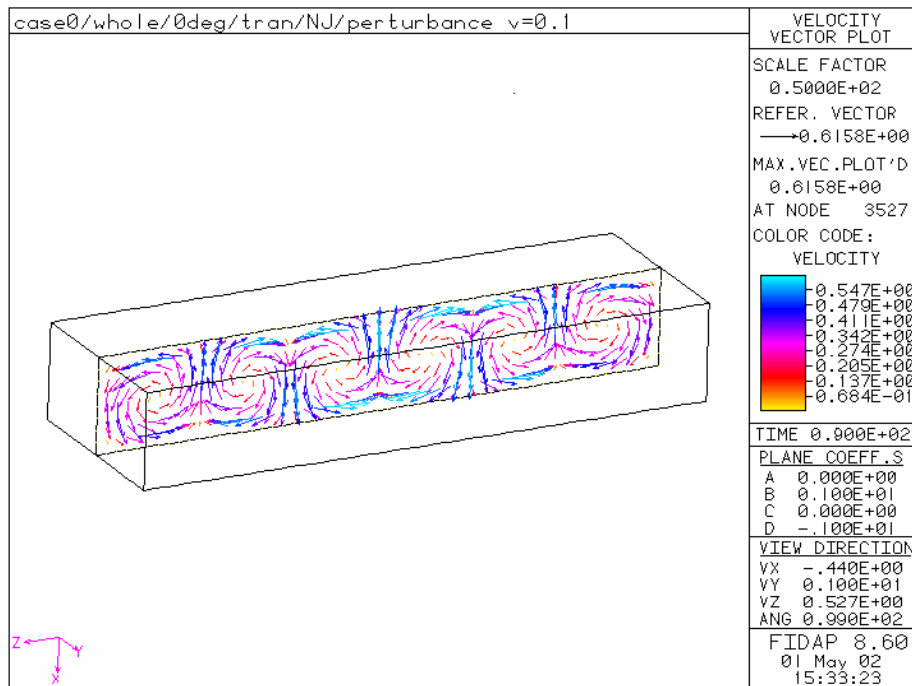


Figure 3. Velocity Vector Plot at Timestep=300 for 6 initial-cells model

The different cell structure resulting from different initial conditions further proved the high sensitivity of the flow to the initial conditions. And also, the cell pattern as well as the number of cells is not steady and changing, which is similar to the observation from Symons and Peck (1984).

Although different initial conditions gave different final flow state, the time-averaged overall Nussel number is almost same. In this case, the Nu at hot wall is about 3.0 for all these different initial conditions.

### 3). Random initial velocity condition.

The overall Nu at hot wall is about 3.0 from applying random initial velocity condition.

### 3.2.2 1x8.4x8.4 cavity, with Ra=12350

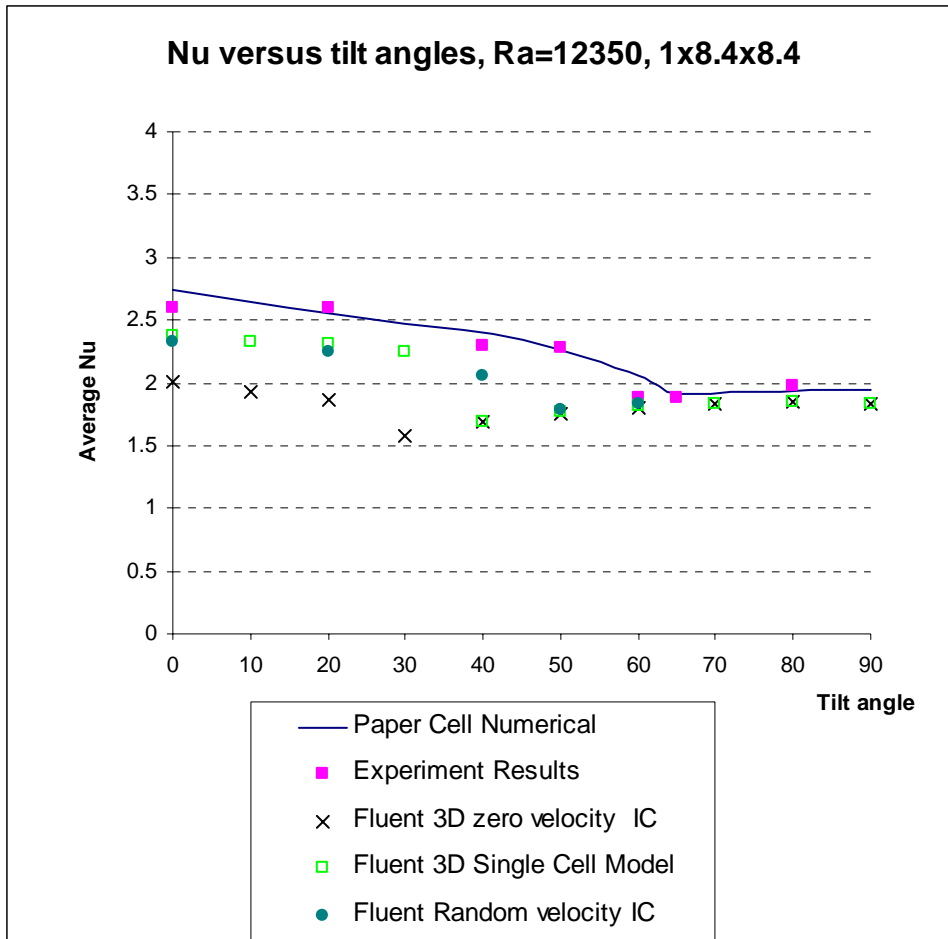


Figure 4. Nusselt Number Results for a Cavity 1x8.4x8.4, Ra=12350

This case is one of those experimental cases from Ozoe et al. (1975), which is a cavity 1x8.4x8.4 and with Ra=12350.

In Fig. 4, Nusselt numbers versus tilt angle were plotted for zero initial velocity condition model, single cell model, and random initial velocity model.

The large discrepancy between the curves of Fluent 3D zero velocity IC and of experiment results might partially be due to the coarse mesh used in Fluent finite-volume calculations. However, it can be seen that Fluent 3D zero IC method under estimates Nu

at every angle below transition angle and predicts Nu over transition angle well. This shows that below transition angle, because of the complex structures inside the flow field, zero velocity initial condition is not a very good representation of the real situation.

Single cell model achieved a better match with the experimental results at small angles. As mentioned before in this report, only when the convection cell size was observed from experiment, can this single cell model be performed, which is the main restriction of this method. And it gave a smaller transition angle at around  $40^\circ$  compared to that from experiment and its difference from the experimental results is obvious to be seen.

Random initial velocity model provided a very close Nu versus tilt angle curve to that of experiment, except for the small deflection of the transition angle. This one might stem from the need for further grid refinement near transition angle because transition might create some important and complex flow structures inside the flow field.

### **3.2.3 1x15.5x15.5 cavity, with Ra=3760**

This case is another one from Ozoe et al. (1975), which is a cavity 1x15.5x15.5 and with Ra=3760.

In Fig. 5, Nusselt numbers versus tilt angle were plotted for random initial velocity model. Because the flow is more complicated at lower inclination angles, the mismatch between the results from this study and Ozoe et al. is more significant. This disagreement is expected to be solved by increasing the grid resolution in the future work. At higher tilt angles, the flow tends to be more two-dimensional and lower grid resolution is able to meet the requirement. One of the major achievement of this case is that transition angle again is predicted correctly to a very good extent. This shows that

Fluent 3D method together with random initial velocity can predict the flow mode transition in a inclined enclosure pretty well.

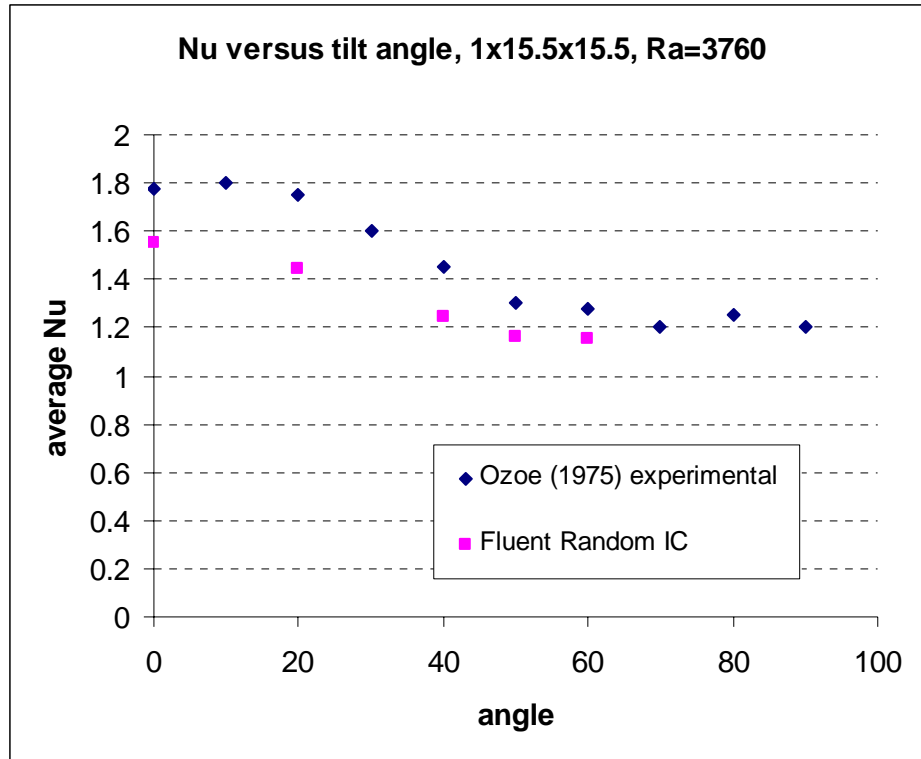
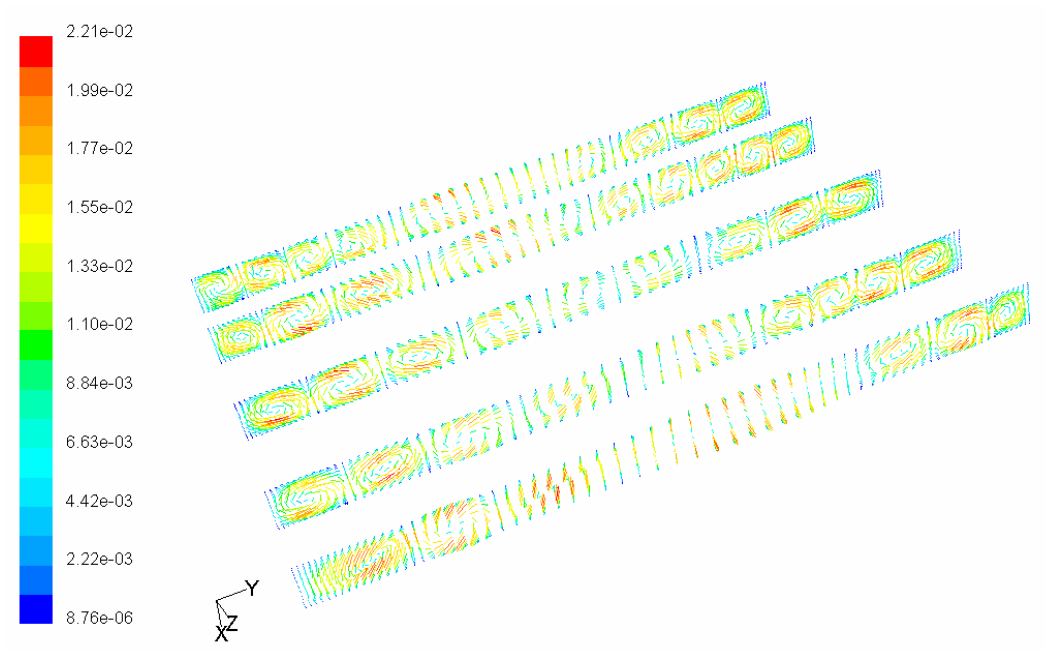


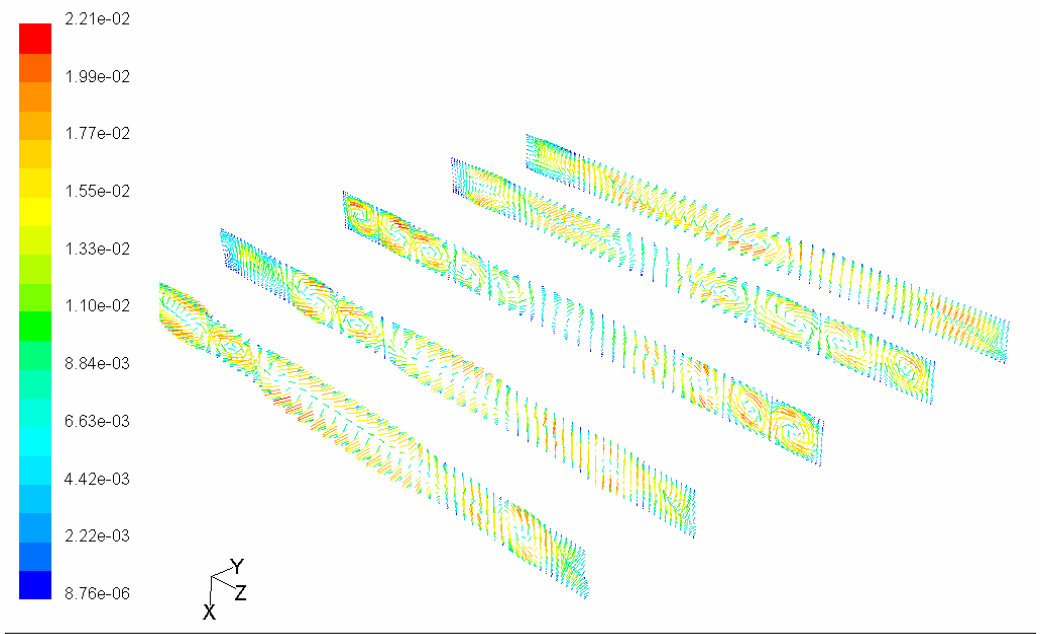
Figure 5. Nusselt number Results for a cavity 1x15.5x15.5, Ra=3760

The velocity vector plots at 0°, 20°, 50°, 60° were shown at Fig. 6, Fig. 7, Fig. 8 and Fig. 9, respectively.



Velocity Vectors Colored By Mean Velocity Magnitude (m/s) (Time=3.3030e+01) Jul 13, 2002  
 FLUENT 6.0 (3d, segregated, lam, unsteady)

**Figure 6a:** Velocity Vector Plot along the z-axis (width direction) at z=0.01, 0.04, 0.08, 0.12, 0.15m.



Velocity Vectors Colored By Mean Velocity Magnitude (m/s) (Time=3.3030e+01) Jul 13, 2002  
 FLUENT 6.0 (3d, segregated, lam, unsteady)

**Figure 6b:** Velocity Vector Plot along the y-axis (height direction) at y=0.01, 0.04, 0.08, 0.12, 0.15m.

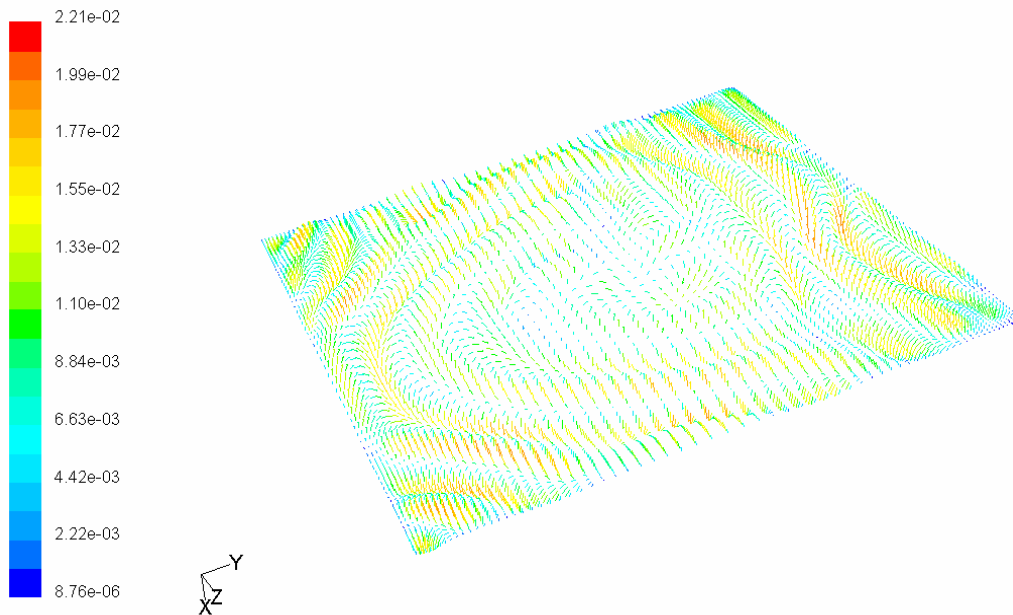


**Figure 6c:** Velocity Vector Plot along the x-axis (length direction) at x=0.005m.  
**Figure 6.** Velocity Vector Plots at angle 0°.

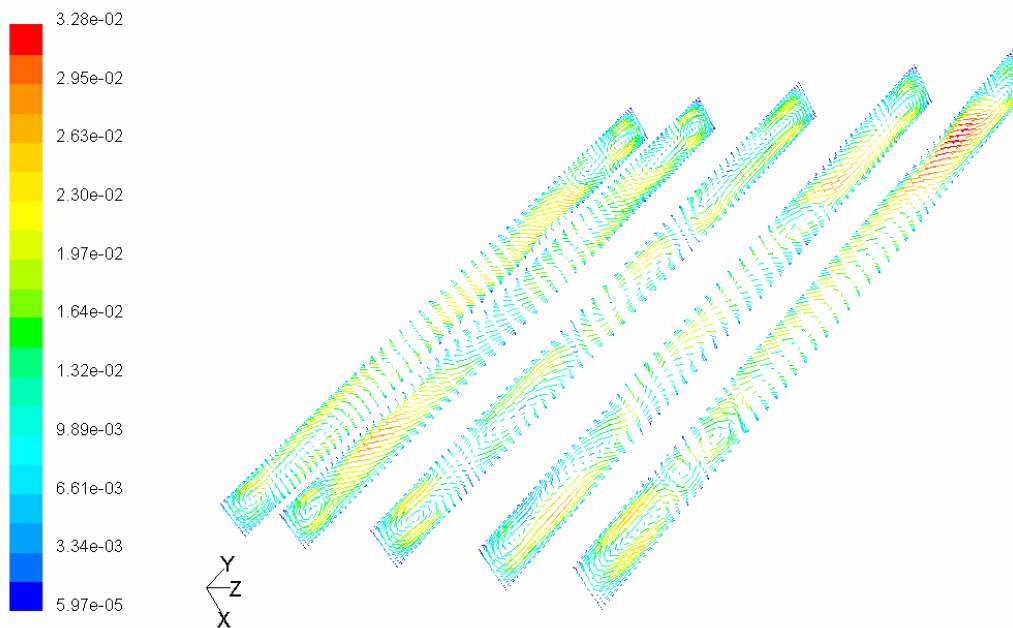
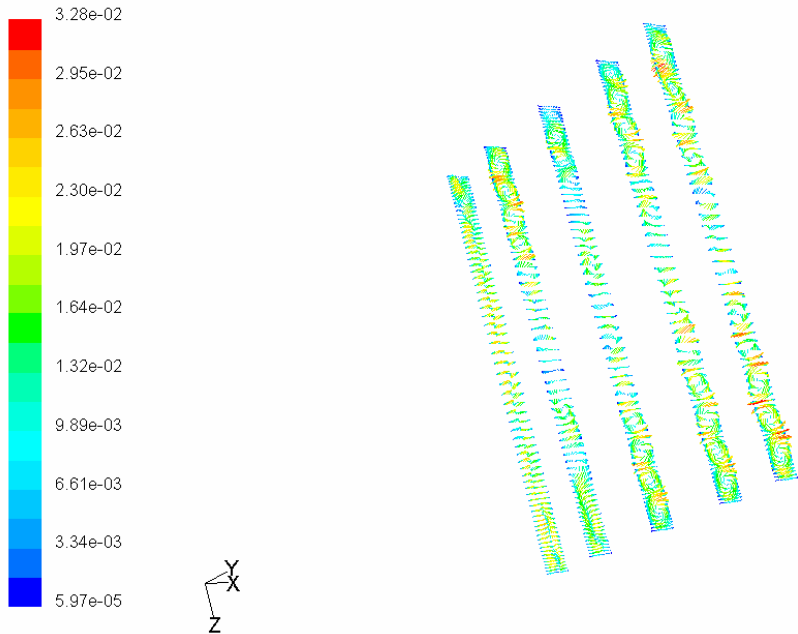
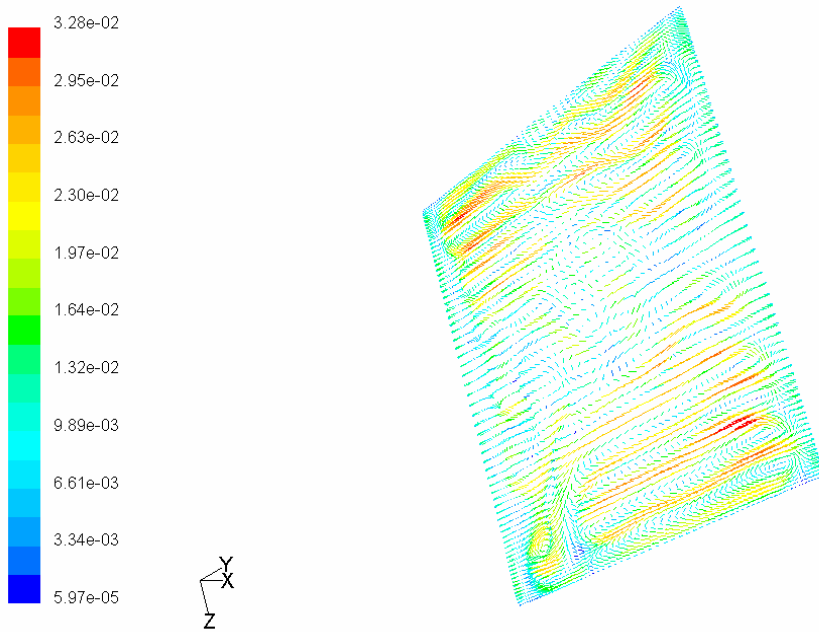


**Figure 7a:** Velocity Vector Plot along the z-axis (width direction) at z=0.01, 0.04, 0.08, 0.12, 0.15m.



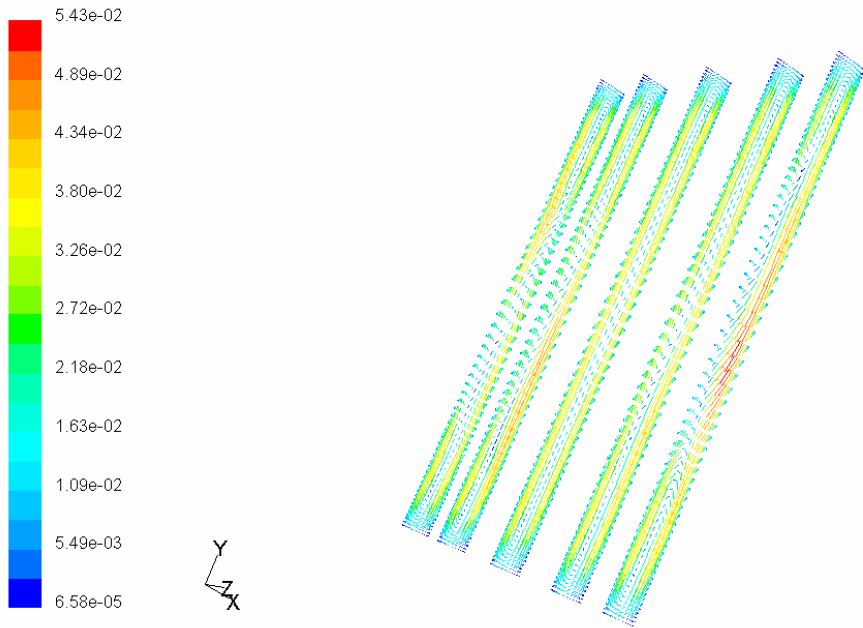
Velocity Vectors Colored By Mean Velocity Magnitude (m/s) (Time=5.1000e+01) Jul 11, 2002  
 FLUENT 6.0 (3d, segregated, lam, unsteady)

**Figure 7b:** Velocity Vector Plot along the y-axis (height direction) at y=0.01, 0.04, 0.08, 0.12, 0.15m.



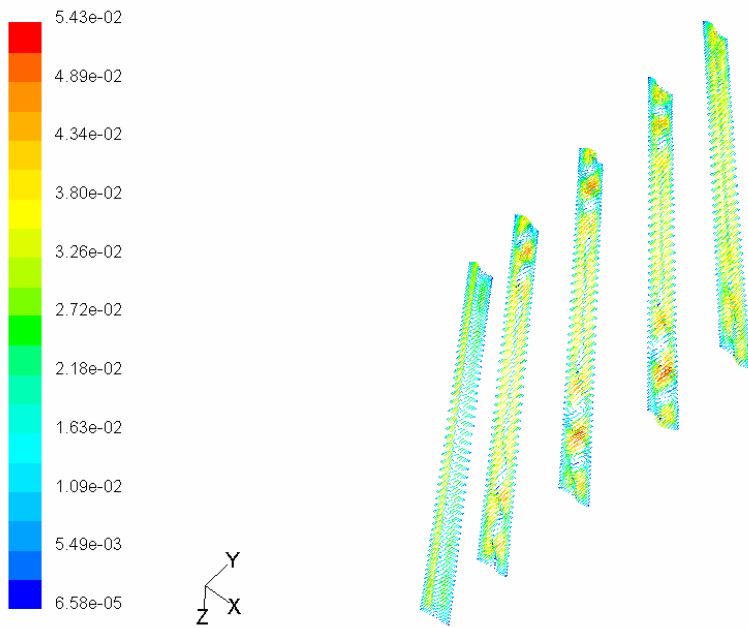
Velocity Vectors Colored By Mean Velocity Magnitude (m/s) (Time=5.1000e+01) Jul 11, 2002  
 FLUENT 6.0 (3d, segregated, lam, unsteady)

**Figure 7c:** Velocity Vector Plot along the x-axis (length direction) at x=0.005m.  
**Figure 7. Velocity Vector Plots at angle 20°.**



Velocity Vectors Colored By Mean Velocity Magnitude (m/s) (Time=3.0000e+01) Jul 10, 2002  
 FLUENT 6.0 (3d, segregated, lam, unsteady)

**Figure 8a:** Velocity Vector Plot along the z-axis (width direction) at z=0.01, 0.04, 0.08, 0.12, 0.15m.



Velocity Vectors Colored By Mean Velocity Magnitude (m/s) (Time=3.0000e+01) Jul 10, 2002  
 FLUENT 6.0 (3d, segregated, lam, unsteady)

**Figure 8b:** Velocity Vector Plot along the y-axis (height direction) at y=0.01, 0.04, 0.08, 0.12, 0.15m.

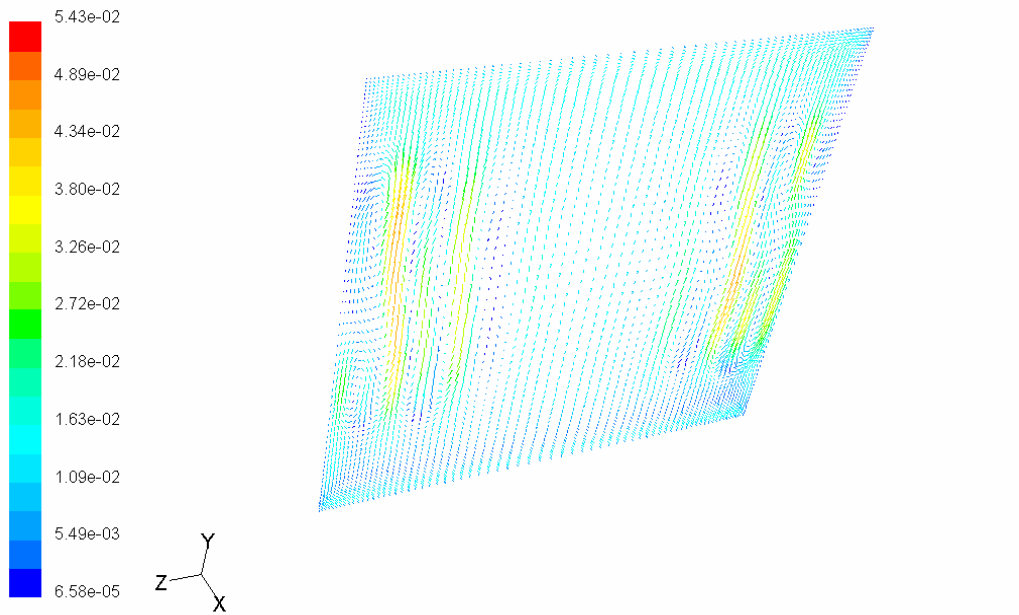


**Figure 8c:** Velocity Vector Plot along the x-axis (length direction) at x=0.005m.  
**Figure 8.** Velocity Vector Plots at angle 50°.

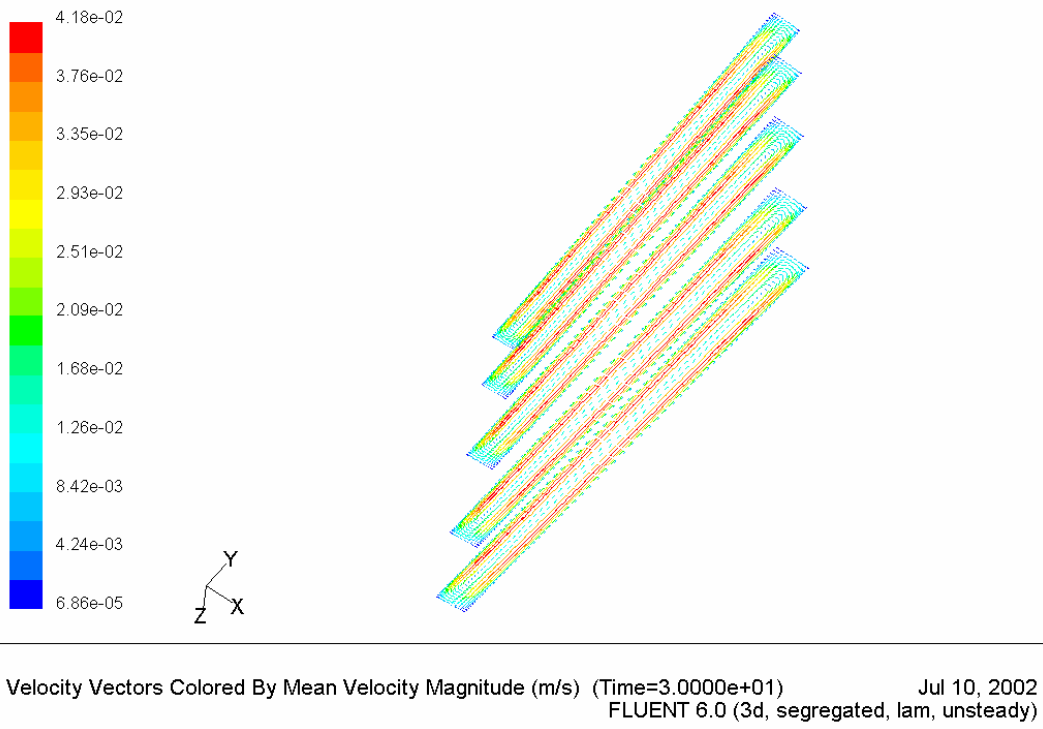


**Figure 9a:** Velocity Vector Plot along the z-axis (width direction) at z=0.01, 0.04, 0.08, 0.12, 0.15m.

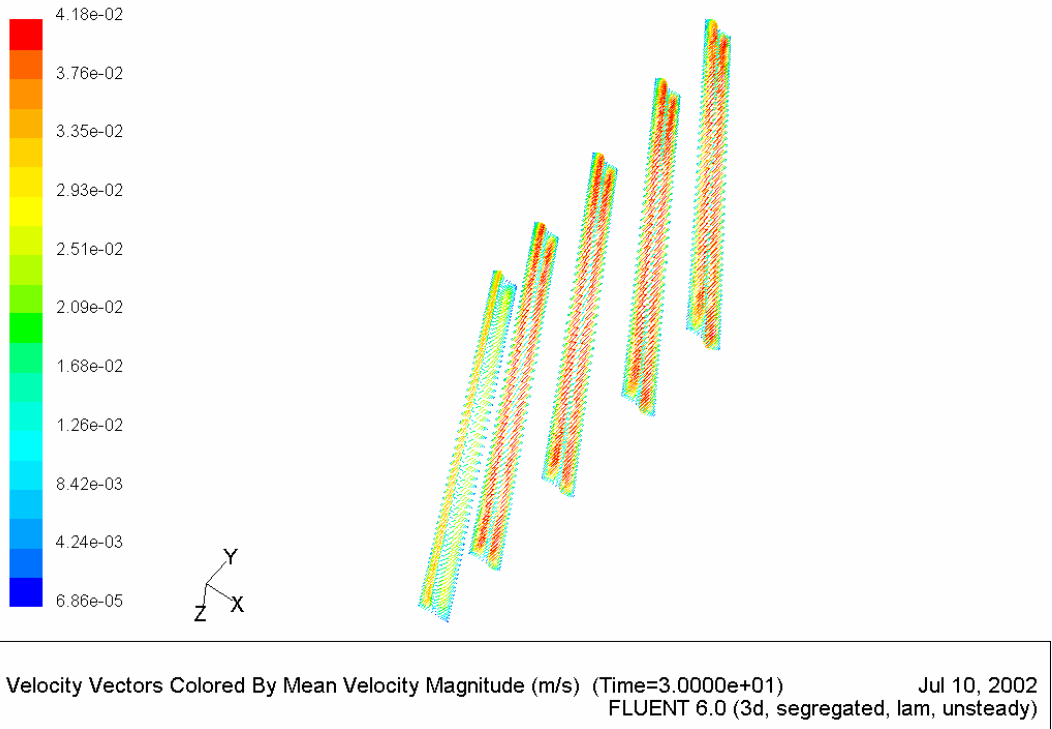


**Figure 9b:** Velocity Vector Plot along the y-axis (height direction) at  $y=0.01, 0.04, 0.08, 0.12, 0.15\text{m}$ .

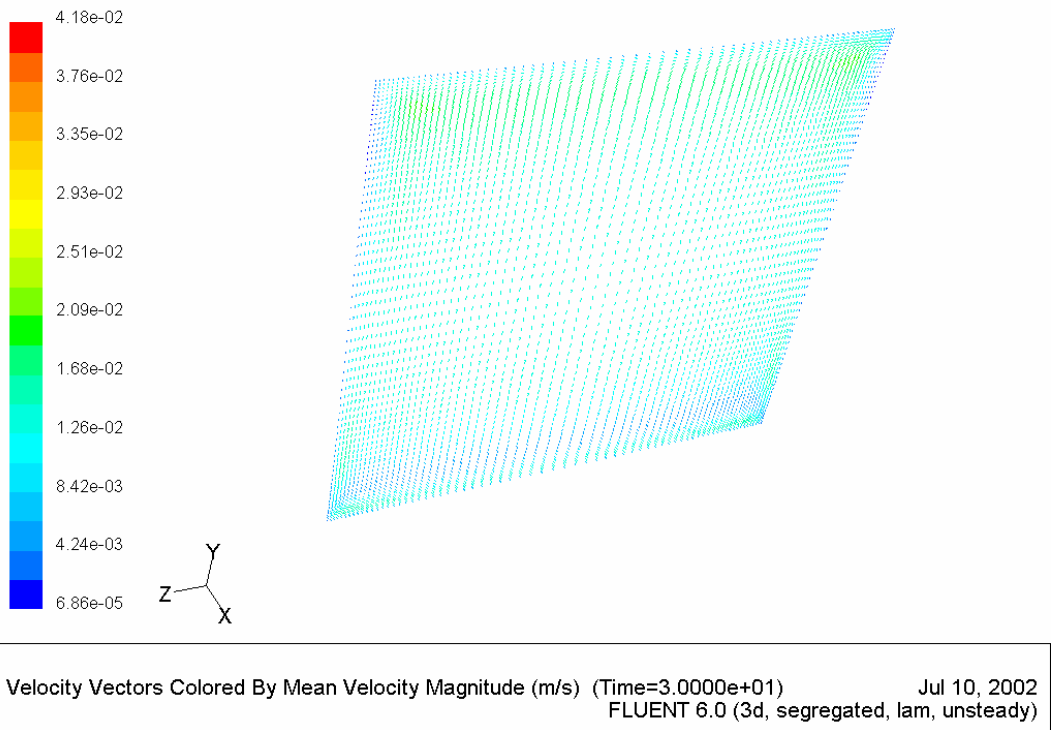


**Figure 9c:** Velocity Vector Plot along the x-axis (length direction) at  $x=0.005\text{m}$ .

**Figure 9.** Velocity Vector Plots at angle  $60^\circ$ .

From the velocity vector plots at different angles above, it can be seen that the flow mode transition occurs somewhere between  $50^\circ$  and  $60^\circ$ . At  $0^\circ$ , there exist rolls with axes in both y-direction and z-direction because the cavity has the same height and width. At  $20^\circ$ , there still exist two groups of convective rolls with perpendicular axes, with the primary convective rolls along y-axis. At  $50^\circ$  just before the transition point, the main circulation flow rising up along the hot wall and going down along the cold wall, already takes its form. But there still exists some secondary small cells with axes along y-direction near the wall area. Also the number of the convective cells near the wall is also decreasing compared to that of  $20^\circ$ . At  $60^\circ$  after the transition point, the flow is almost two-dimensional, with only very tiny 3-D effect near the corner, which doesn't influence the local heat transfer too much.

## **4 Future Work**

Three-dimensional simulation is the necessary way to numerically predict correct heat transfer results of buoyancy inclined cavity flow. Because of the sensitivity to the initial conditions, the choice of using the appropriate initial conditions to give the flow field a suitable perturbation is important. Based on the calculations so far, applying random initial velocity conditions is a promising method. Three cases of validation of such method provided acceptable heat transfer results and the flow mode transition angles. Further work on grid resolution analysis and numerical scheme refinement may lead to better results.

More validation needs to be performed on cavities with higher aspect ratios. Several cases from Elsherbiny et al. (1982) will be simulated as validation for random initial velocity model so that it can be used for higher aspect ratio cases.

Also, some further 3-D mesh study needs to be done to establish a good meshing method.

After validation performed, a real glazing cavity will be simulated.

## 5 Reference:

- Elsherbiny, S.M., G.D. Raithby, K.G.T. Hollands. 1982. Heat Transfer by Natural Convection across Vertical and Incline Air Layers. *Transactions of the ASME*. 96/ Vol. 104, Feb.
- Ozoe, H., H. Sayama and S. W. Churchill. 1975. Natural Circulation in an Inclined Rectangular channel at Various Aspect Ratios and Angles—experimental Measurements. *International Journal of Heat and Mass Transfer*. Vol. 18, pp.1425-1420.
- Ozoe, H. and K. Fujii. 1983. Long Rolls Generated by Natural Convection in an Inclined, Rectangular Enclosure. *International Journal of Heat and Mass Transfer*, v 26, n 10, Oct, 1983, pp 1427-1438.
- Symons, J.G. and M.K. Peck. 1984. Natural Convection Heat Transfer Through Inclined Longitudinal Slots. *Transactions of the ASME*, v 106, Nov 1984, pp 824-829.
- Yang, H. Q., K. T. Yang and J. D. Lloyd. 1986. Flow Transition in Laminar Buoyant Flow in a Three-dimensional Tilted Rectangular Enclosure. *Proceedings of the International Heat Transfer Conference*, v 4, 1986.
- Yang, K. T. 1988. Transitions and Bifurcations in Laminar Buoyant Flows in Confined Enclosures. *Journal of Heat Transfer*, v 110, Nov 1988, pp 1191-1204.